Journal of Materials Chemistry A

Accepted Manuscript

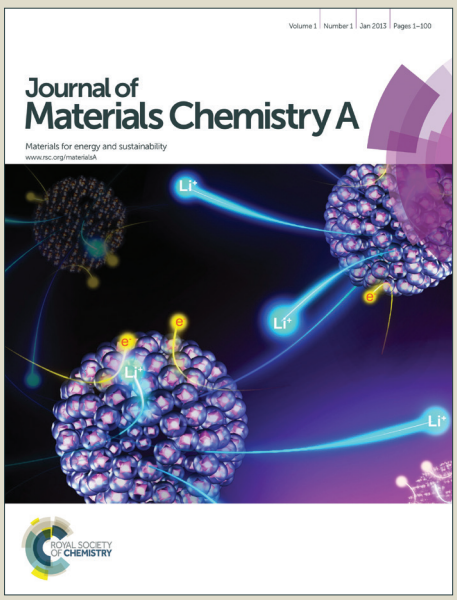

ROYAL SOCIETY OF CHEMISTRY

www.rsc.org/materialsA

Journal Name

RSCPublishing

ARTICLE

Tetragonal vs. cubic phase stability in Al – free Ta doped $Li_7La_3Zr_2O_{12}$ (LLZO)

Cite this: DOI: 10.1039/xoxxoooooox

Travis Thompson[a], Jeff Wolfenstine[b], Jan L. Allen[b], Michelle Johannes[c], Ashfia Huq[d], Isabel N. David[a], and Jeff Sakamoto[a]

Received ooth January 2012,
Accepted ooth January 2012

DOI: 10.1039/xoxxoooooox

www.rsc.org/

$Li_7La_3Zr_2O_{12}$ (LLZO) garnet is attracting interest as a promising Li-ion solid electrolyte. LLZO exists in a tetragonal and cubic polymorph where the cubic phase exhibits ~2 orders of magnitude higher Li-ion conduction. It has been suggested that a critical Li vacancy concentration (0.4 – 0.5 atoms per formula unit) is required to stabilize the cubic polymorph of $Li_7La_3Zr_2O_{12}$. This has been confirmed experimentally for Al^{3+} doping on the Li^+ site. Substitution of M^{5+} (M = Ta, Nb) for Zr^{4+} is an alternative means to create Li vacancies and should have the same critical Li vacancy concentration, nevertheless, subcritically doped compositions (0.25 mols of Li vacancies per formula unit) have been reported as cubic. Advantageous Al, from alumina crucibles, was likely present in these studies that could have acted as a second dopant to introduce vacancies. In this work, Al-free subcritically doped ($Li_{6.75}La_3Zr_{1.75}Ta_{0.25}O_{12}$) and critically doped ($Li_{6.5}La_3Zr_{1.5}Ta_{0.5}O_{12}$) compositions are investigated. X-ray diffraction indicates that both compositions are cubic. However, upon further materials characterization, including SEM analysis, Raman spectroscopy, Electrochemical Impedance Spectroscopy, and neutron diffraction it is evident that the subcritically doped composition is a mixture of cubic and tetragonal phases. The results of this study confirm that 0.4 - 0.5 Li vacancies per formula unit are required to stabilize the cubic polymorph of LLZO.

Introduction

There is interest in the garnet $Li_7La_3Zr_2O_{12}$ (LLZO), discovered by Weppner *et al.*[1] as a Li-ion conducting solid electrolyte for use in Li/Li-ion solid-state, Li-air and Li-sulfur batteries because of its stability against metallic Li, moderate stability in air, and high lattice conductivity (~0.2 x 10^{-3} to 1 x10^{-3} S/cm) at room temperature for the cubic structure[1-4]. LLZO can also exist with a tetragonal structure[5,6]. The conductivity of the tetragonal phase at room temperature is ~2 orders of magnitude lower than that for the cubic phase[6,7]. Thus, the challenge has been to stabilize the cubic phase of LLZO. It was found experimentally that 0.2 – 0.24 mols of Al substitution (0.4 – 0.48 Li vacancies) per formula unit in LLZO stabilized the cubic phase[8]. Subsequently, combination density functional and molecular dynamics computations suggested that a critical Li vacancy concentration in the range 0.4 – 0.5 per LLZO formula unit, regardless of how the vacancies are introduced, is required to stabilize the cubic phase[9]. One method to achieve the critical Li vacancy concentration and hence, stabilize cubic LLZO, is through the substitution of super valent cations such as Al[8,10], Ga[11], Fe[12] for Li, and / or Nb[2,13], Ta[14,15], Sb[16] for Zr which results in the formation of Li vacancies to balance the extra positive charge of the super valent cation. The critical Li vacancy concentration predicted by computation for cubic LLZO agrees well with experimental results required to obtain cubic LLZO when substitution is performed on the Li sublattice, for $Li_{7-3x}M_xLa_3Zr_2O_{12}$ where the critical amount of M= Al ($x \approx 0.2$)[8], Ga ($x \approx 0.2$)[11] and Fe ($x \approx 0.19$)[12]. Since the dopant resides on the Li site, only two Li vacancies are created even though three Li atoms are expelled. In contrast for the case of Nb[2,13], Ta[14,15], Sb[16], where the substitution is performed on the Zr site, it has been reported that the cubic phase is obtained for $Li_{7-y}La_3Zr_{2-y}M_yO_{12}$ (where M=Nb, Ta, Sb) for y as low as $y \approx 0.2$. This is about 2 times lower than the critical amount (y = 0.4 – 0.5) predicted. Thus, there is good agreement between predictions when super valent cation substitution is performed for Li, while there is disagreement when the super valent substitution is performed for Zr. One possible reason is that the heat-treatment was performed in alumina crucibles for samples where the super valent cations (Nb, Ta, Sb) were substituted for Zr[2,13-16]. Thus, there is the possibility that Al entered the lattice[17] in addition to the intentional doped super valent cation and hence, the actual Li vacancy concentration is higher than expected. Since Al substitution on a Li site creates twice as many lithium vacancies compared to substitution of a M^{5+} (such as Nb, Ta and Sb) on a Zr site (Kröger-Vink notation: $2[Al_{Li}^{\bullet\bullet}] = [V_{Li}^{\prime}]$ vs. $[M_{Zr}^{\bullet}] =$

$[V'_{Li}]$), a small amount of extra Al can make a large difference on the actual vacancy concentration and the resulting phase. As a result this study was undertaken to determine if our previous experimental observations for Al substitution[8] and the computations of Bernstein *et al.*[9] correctly predict the stability of tetragonal versus cubic phase for the case of super valent doping on the Zr site without the presence of Al. In this work Ta^{5+} was selected as the super valent dopant owing to its comparable ionic radius[18] and the creation of Li vacancies when substituting for Zr^{4+}. Al uptake into the LLZO samples was prevented since no alumina labware was used in any of the processing steps. In this study, the nominal compositions $Li_{6.75}La_3Zr_{1.75}Ta_{0.25}O_{12}$ and $Li_{6.5}La_3Zr_{1.5}Ta_{0.5}O_{12}$ were investigated. The Ta = 0.25 composition was selected because it is less than the critical Li vacancy concentration predicted to stabilize the cubic phase. This composition has been shown to be the composition with maximum conductivity in a related LLZO series where the Nb^{5+} ion was used[2,13]. The Ta = 0.5 composition was selected because it is at or near the critical Li vacancy concentration predicted to stabilize the cubic phase[9]. This work used several materials characterization techniques, including X-ray diffraction, SEM analysis, Raman spectroscopy, electrochemical impedance spectroscopy and neutron diffraction to investigate the tetragonal versus cubic phase stability as a function of Li vacancy concentration.

Experimental

Samples of compositions $Li_{6.5}La_3Zr_{1.5}Ta_{0.5}O_{12}$ and $Li_{6.25}La_3Zr_{1.75}Ta_{0.25}O_{12}$ were prepared using a co-precipitation process. Li_2CO_3, $La(OH)_3$, "$[ZrO_2]_2CO_2{\bullet}xH_2O$" (zirconium carbonate, basic hydrate; equivalent ZrO_2 content determined from thermogravimetric analysis) weighed in the desired stoichiometry were dissolved in ~1.4 M HNO_3 (aq). A 6 wt. % excess of Li was used to compensate for Li volatilization during synthesis. The stoichiometric amount of $TaCl_5$ was first dissolved in anhydrous ethanol and then added to the Li, La and Zr containing precursor solution. The resulting solution was evaporated to dryness in a microwave oven contained inside a fume hood. Evolution of NO_x was observed during this step. The dried co-precipitate was lightly ground with a mortar and pestle and pressed into a pellet using a Carver laboratory die and press. The pellet was placed on a ZrO_2 plate and heated in air at 1173 K for 3-4 h. The furnace was turned off and the sample was removed.

The powders were consolidated by Rapid Induction Hot-pressing (RIHP) at 1323 K and 62 MPa for 1 hr in graphite dies in air under argon shielding gas. The density of each sample was calculated using the bulk geometry and the mass.

Powder X-ray diffraction data were collected at room temperature on a Rigkau MiniFlex 300 using Cu Kα radiation over 10 - 120 degrees 2θ range with a 0.03 degrees step size and 12 seconds per point. A reference pattern for the cubic structure was taken from the ICSD database[15], which had a Ta content of Ta = 0.55.

SEM was performed on a Carl Zeiss Auriga Cross-Beam FIB-FESEM at an accelerating voltage of 15 kV and a working distance of 6.9 mm. 5nm of Pt was sputtered to prevent charging because it is not reactive with Li. The grain size was estimated from the SEM micrographs of the fracture surface using the linear intercept method.

Raman spectra were collected with a Renishaw inVia Raman microscope using a 532 nm laser, 2400 lines/mm holographic grating and 50x magnification. The intensities were normalized to the maximum value. Raman spectroscopy is spot analysis. With the optics used in this experiment, the laser spot size was ~5 microns while the average grain size (see SEM analysis below) was ~1.4 microns. Since each scan samples a few grains, spectra were collected at ~5 random locations several millimetres apart on the RIHPed pellet and the normalized intensities averaged together so that the result was more representative of the bulk sample. The uncertainty in the averaged intensity values was estimated using the standard error of the mean. An undoped tetragonal composition with the nominal formula $Li_7La_3Zr_2O_{12}$ was prepared for reference.

Electrochemical impedance spectroscopy (EIS) was performed with a Bio-Logic SP200 from 10Hz to 7MHz with a 100mV perturbation amplitude and sputtered Pt blocking electrodes at room temperature. The impedance spectra were modelled using a modified equivalent circuit proposed by Huggins[19].

Time of flight neutron powder diffraction data were collected at 300K at the POWGEN beamline at the Spallation Neutron Source (SNS), Oak Ridge National Laboratory (ORNL) with center wavelengths of 1.066Å and 2.655Å at 300K to obtain diffraction patterns that spans from d-spacing of 0.3Å to 6.2Å.

Results and Discussion

X-ray diffraction

X-ray diffraction (XRD) was conducted on the two compositions and is shown in Figure 1.

Both diffraction patterns exhibit the cubic garnet structure with trace impurities. As reported by other groups for Nb[2,13], Ta[14,15], Sb[16], both the critically doped ($Li_{6.5}La_3Zr_{1.5}Ta_{0.5}O_{12}$) and subcritically ($Li_{6.25}La_3Zr_{1.75}Ta_{0.25}O_{12}$) doped compositions appear to be cubic from the XRD. However, these reports likely had Al present as previously discussed. In this work, the observance of the cubic structure with XRD for the critically doped composition is in agreement with what is predicted. However, the observance of the cubic XRD pattern for the Al - free subcritically doped composition ($Li_{6.25}La_3Zr_{1.75}Ta_{0.25}O_{12}$) was unexpected since there should be insufficient Li vacancies. In order to further investigate the structure of Al - free sub-and critically doped LLZO garnet the sample powders were hot-pressed and further materials characterization was performed.

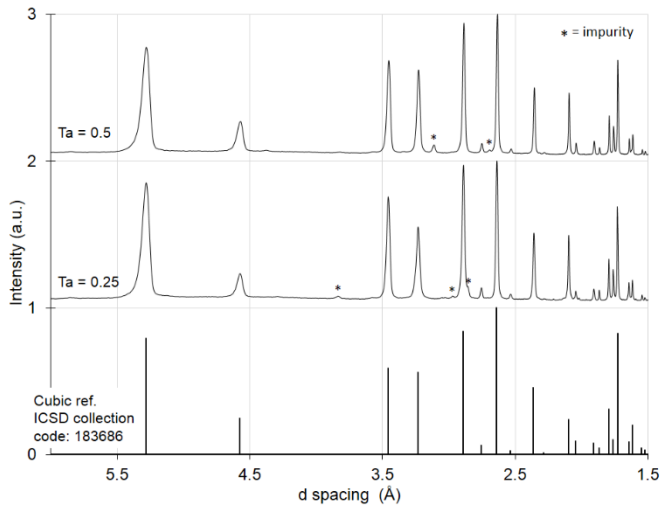

Figure 1: X-ray diffraction of the critically doped composition $Li_{6.5}La_3Zr_{1.5}Ta_{0.5}O_{12}$, the subcritically doped composition $Li_{6.75}La_3Zr_{1.75}Ta_{0.25}O_{12}$, and a cubic reference[15]. Peaks corresponding to impurities are marked by (*).

SEM analysis

After hot pressing the powders, SEM analysis was performed on fracture surfaces of the nominal compositions $Li_{6.75}La_3Zr_{1.75}Ta_{0.25}O_{12}$ and $Li_{6.5}La_3Zr_{1.5}Ta_{0.5}O_{12}$ to characterize the fracture mode, grain size, and porosity (Figure 2).

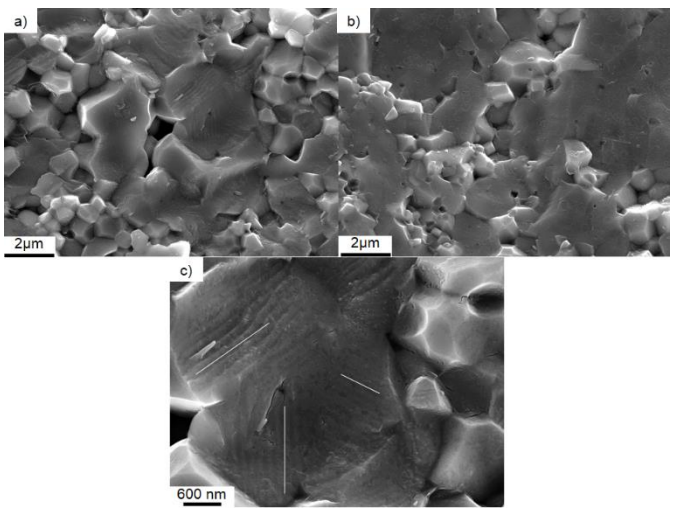

Figure 2: SEM micrographs of the fracture surface of hot-pressed pellets of a) the subcritically doped composition $Li_{6.75}La_3Zr_{1.75}Ta_{0.25}O_{12}$ and b) the critically doped composition $Li_{6.5}La_3Zr_{1.5}Ta_{0.5}O_{12}$. Panel c) shows a higher magnification micrograph of the striations observed in the subcritically doped composition. Lines were added to highlight the striations observed.

Since structural refinement of the diffraction data is still underway, the theoretical density for the two compositions was estimated from the nominal compositions and the lattice parameters of Logéat[15] *et. al.* However, it should be noted that the lattice parameter in the work of Logéat *et. al.* was determined under the assumption of a single, cubic phase present. Both samples had relatively dense microstructures (~98% for both compositions) with similar microstructural features; an average grain size of 1.4 microns and a mixed inter- and transgranular fracture mode. The relatively dense micrographs, similar grain sizes, and fracture mode indicate that Ta – doped LLZO samples without Al can be consolidated close to the theoretical density without the use of a sintering aid. Striations were observed in some of the grains in the subcritically doped composition (Figure 2 b and c). We have previously reported similar striations in tetragonal LLZO which was consolidated using the same technique[6]. These striations were not present in any of the grains for the critically doped composition. We believe the striations result from a twinning phenomenon as described by Wolfenstine *et al.*[6] and are an indicator of the tetragonal phase. Since these striations were only observed in some, but not all, of the grains of the subcritically doped composition, this is taken as evidence that the sample is a mixture of cubic and tetragonal phases. Since the subcritically doped composition appears to be a mixture of cubic and tetragonal phases in SEM, yet cubic in XRD, Raman spectroscopy was performed to further clarify the results.

Raman Spectroscopy

The Raman spectra shown in Figure 3 were collected for each sample. The line represents the average intensity value of the ~5 locations while the black region of varying width around the line represents the uncertainty in the intensity.

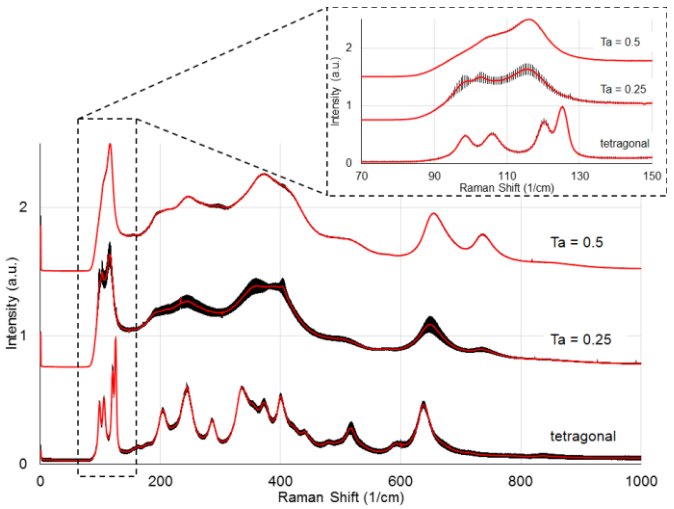

Figure 3: Average Raman spectra and estimated uncertainty in the intensity (black region of varying width) for the subcritically doped composition $Li_{6.75}La_3Zr_{1.75}Ta_{0.25}O_{12}$, the critically doped composition $Li_{6.5}La_3Zr_{1.5}Ta_{0.5}O_{12}$, and a tetragonal reference. The inset shows a magnification of the bands near 110 cm^{-1}. The uncertainty in the intensity was estimated by the standard error of the mean.

Since there are many overlapping features in the Raman spectra and the sample analyzed was polycrystalline, deconvolution of the spectra is not possible and this analysis will be limited to qualitative observations. Preliminary investigations of the Raman spectra of LLZO have been reported by Tietz *et al.*[20] They reported that the band near 650 cm^{-1} is related to the stretching of the ZrO_6 octahedra[20]. Several observations can be made from the Raman spectra in Figure 3.

First, there is an additional band near 750 cm^{-1} which appears and grows in intensity as more Ta is added to the system. Since bands in this region correspond to stretching of the ZrO_6 octahedron, the appearance of the band at 750 cm^{-1} as Ta is added to the system corresponds to stretching of TaO_6 octahedron.

Second, the ratio of the intensities of these two bands (~650 cm^{-1} and ~750cm^{-1} for the Zr and Ta respectively) is a function of the Ta content in the garnet. Any uncertainty in the intensity of either of the bands at ~650 cm^{-1} or ~750cm^{-1} means there is also an uncertainty in the ratio of these bands. Since the intensity plotted in Figure 3 is an average of ~5 points across the sample and the Raman spot size samples a few grains per point, uncertainty in the band intensity ratio suggests that the Ta content varies from point to point.

Third, for the subcritically doped composition, there is considerable uncertainty in the intensity ratio of the bands at ~650 cm^{-1} and ~750cm^{-1}. As argued above, this suggests that there is variation in the Ta content at different points in the subcritical sample. This is in contrast to the critically doped composition where there is little uncertainty in the intensity ratio of the bands at ~650 cm^{-1} and ~750cm^{-1}, suggesting a uniform Ta concentration throughout the sample. Since it is expected that the Ta content of the tetragonal phase would be different than the cubic phase, variation of the band intensity ratio in the subcritically doped composition would be consistent with the SEM analysis which suggested that the microstructure segregated into tetragonal and cubic phases.

Fourth, if the compositional uncertainty in the subcritically doped sample is due to the microstructure phase segregation into cubic and tetragonal regions, then some direct evidence of the tetragonal phase should be present in the spectra. A reduction of symmetry from cubic to tetragonal will result in splitting of the vibrational modes. Tietz *et al.*[20] showed that this is most evident in the bands near ~110 cm^{-1}. The inset in Figure 3 shows a magnification of this region. It is evident that the subcritically doped composition (Ta = 0.25) is a superposition of the tetragonal reference and the critically doped spectra with clear splitting of the bands. This observation is especially evident when the uncertainty in the intensity is considered. This confirms that the subcritically doped sample is not single phase cubic but a mixture of cubic and tetragonal phases.

It is important to note that the spot size for the Raman analysis is ~3.5x that of the average grain size. As such, several grains are being sampled at each location. This could include any impurities present in either of the doped compositions or the tetragonal control. Indeed, trace impurities, likely with a perovskite structure, are visible in the XRD (marked in Figure 1). Since the intensity of these peaks are minor relative to that of the LLZO, the impurities are not expected to change the interpretation of the diffraction results. However, these impurities could manifest as additional bands in the Raman spectra. Since so many vibrational modes are active and overlapping for the LLZO and secondary phases, such as those with the perovskite like structure, could be present as well, it is difficult to assign the bands to particular vibrational modes. As such, electrochemical impedance spectroscopy with equivalent circuit modeling was performed to help clarify the results of the Raman Spectroscopy and SEM analysis.

Electrochemical Impedance Spectroscopy

Since the density and grain size are similar, comparison of the transport properties is possible. As a consequence, EIS was performed on the two compositions and equivalent circuit modeling of the data was performed. Figure 5 shows the Nyquist plot of the EIS data at room temperature, the equivalent circuit, and the modeled impedance response.
The capacitors in the Huggins model were replaced with constant phase elements (CPEs) to account for any dispersion in the time constants. The complex impedance response of a single CPE is given by:

$$Z(\omega) = \frac{1}{Q(j\omega)^{\alpha}}$$

where $Z(\omega)$ is the frequency dependent impedance, ω is the frequency, j is the imaginary operator, Q is related to the capacitance and α is the ideality coefficient.

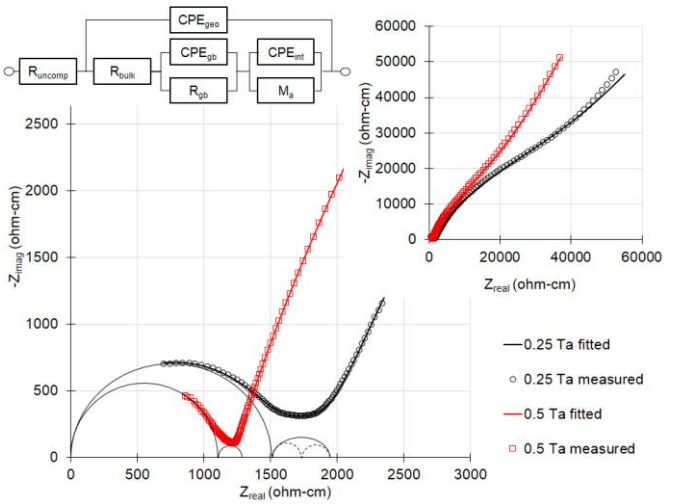

Figure 4: Nyquist plot of the complex impedance calculated from the EIS measurement performed at room temperature. The open symbols correspond to the experimental data and the solid lines are the fitted results of the equivalent circuit. The equivalent circuit model is shown in the top left. The inset shows the low frequency portion of the spectra. The semi-circles are included to help guide the eye.

The values of Q for a CPE should be on the order of ~10^{-12} F/cm^2 for the bulk and ~10^{-9} F/cm^2 for the grain boundaries[19,21]. The refined CPE Q values from the equivalent circuit modeling for the bulk and grain boundary processes for both compositions agree with the expected Q values for these physical processes. The ideality of the CPE is represented by the coefficient α. The values for the ideality coefficient α were allowed to refine and settled to values near 1 for the bulk process for both compositions. For the critically doped composition, the α value for the grain boundary feature also refined to nearly 1. However, for the subcritically doped

composition, the α value was 0.78 and the resulting semi-circular feature was depressed. A depression in the mid-frequency regime has been observed for tetragonal LLZO, which also exhibited a twinned microstructure[6]. Since twinning and grain boundaries are both two dimensional defects, they have similar capacitances[22,23]. Consequently, it is likely that the low α value for the mid-frequency CPE element for the subcritically doped composition is caused by the presence of more than one defect, namely the twinned tetragonal grains and grain boundaries. Analysis of the EIS data, therefore, suggests that the subcritically doped sample is not single phase cubic but a mixture of cubic and tetragonal phases. In contrast, the EIS data for the critically doped sample is as expected for purely cubic LLZO.

Neutron Diffraction

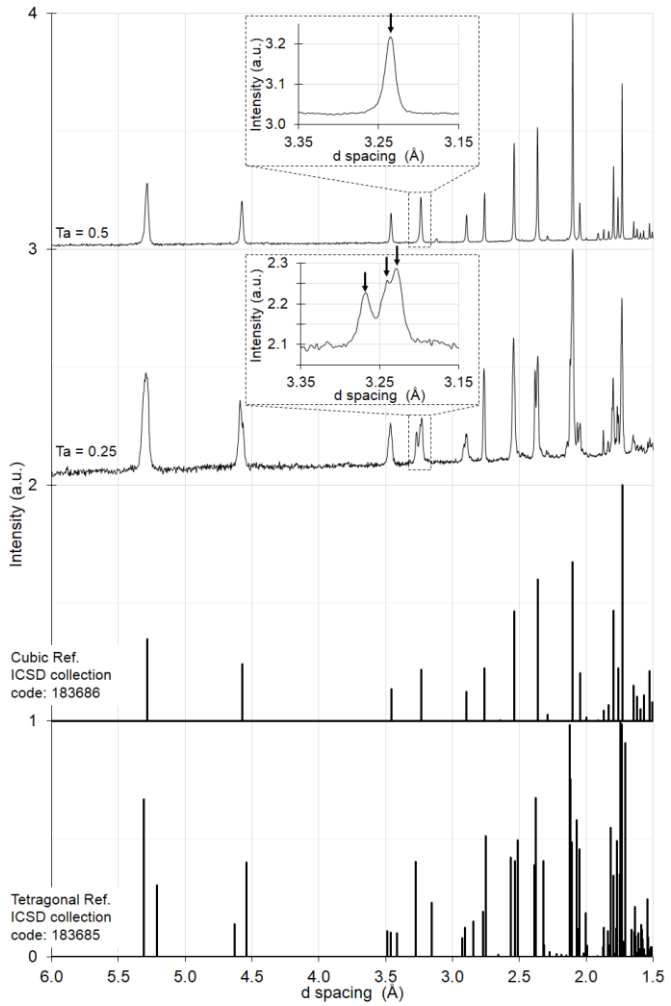

Figure 5: Neutron diffraction of the critically doped composition $Li_{6.5}La_3Zr_{1.5}Ta_{0.5}O_{12}$, the subcritically doped composition $Li_{6.75}La_3Zr_{1.75}Ta_{0.25}O_{12}$, a cubic reference[15], and a tetragonal reference[15]. The insets highlight the (400) peak splitting observed.

The SEM, Raman, and EIS analysis do not support the observation made in the XRD that both the sub- and critically doped compositions are entirely cubic. It should be noted, however, that lab scale diffraction experiments can be resolution limited. Furthermore, XRD is insensitive to light elements and the tetragonal distortion results from ordering on the Li sublattice. Because of the sensitivity to Li, high resolution neutron diffraction (ND) was performed at the POWGEN beamline of the Spallation Neutron Source at Oak Ridge National Laboratory. Structural refinement of the sub- and critically doped compositions, as well as additional dopant concentrations, is under way and not presented here. As such, this analysis is treated qualitatively to confirm the observations made in the SEM, Raman, and EIS analysis. The ND patterns for the sub- and critically doped compositions are shown in Figure 5. The ND pattern of the critically doped composition, $Li_{6.5}La_3Zr_{1.5}Ta_{0.5}O_{12}$, shows single peaks for each Bragg reflection, indicating that the phase is cubic. However, the ND pattern for the subcritically doped composition, $Li_{6.75}La_3Zr_{1.75}Ta_{0.25}O_{12}$, clearly shows peak splitting. The insets in Figure 5 show the single (400) peak at a d spacing of 3.23 Å of the critically doped cubic LLZO composition and highlights the splitting of the sample peak for the subcritically doped composition into three peaks. Splitting of the peaks has been observed in undoped tetragonal compositions[6] and for subcritical Al doping on the Li site[10] in XRD. If only the tetragonal phase was present, then it would be expected that the single peak would split into two. However, since three peaks are observed, the high resolution ND supports the observations made in the SEM, Raman, and EIS analysis that the subcritically doped composition, $Li_{6.75}La_3Zr_{1.75}Ta_{0.25}O_{12}$, is a mixture of cubic and tetragonal phases.

In summary, since the XRD showed both the subcritically doped and the critically doped compositions as cubic, further materials characterization was performed. First, SEM analysis of the subcritically doped composition showed distinct striations in the microstructure where there were none in the microstructure of the critically doped composition. Second, Raman spectra of the subcritically doped composition showed variation in the Ta content from point to point and splitting of the vibrational modes where no variation in the Ta content nor splitting of the vibrational modes were observed in the critically doped composition. Third, EIS analysis showed a clear depression of the mid-frequency feature in the Nyquist plot of the subcritically doped composition and exhibited an α value of 0.78 for the CPE element where the mid-frequency feature for the critically doped composition was nearly ideal and exhibited an α value of 0.98 for the CPE. Finally, high resolution ND of the subcritically doped composition clearly showed splitting of the Bragg reflections while the critically doped composition did not. The results of the neutron diffraction data are in excellent agreement with the SEM, Raman, and EIS analysis and confirm that the subcritically Ta doped composition is a mixture of tetragonal and cubic phases while the critically Ta doped composition is entirely cubic. Furthermore, this is in agreement with experimental observations with Al doping[8] and combination density functional and molecular dynamics computations[9] which predict that a critical doping level of 0.4 – 0.5 Li vacancies per formula unit is required to stabilize the

cubic phase. The previous discrepancies between prediction and the experimental results for super valent cation doping on the Zr site may be a result of Al incorporated during the processing steps. Finally, this work suggests that SEM and Raman analysis can complement X-ray diffraction to detect the presence of the tetragonal phase in compositions very near the critical doping level. This is important since nearly all of the highest conductivities have been reported at Li vacancy concentrations close to 0.4 - 0.5 vacancies per formula unit.

Conclusions

This study was designed to determine the critical doping concentration of supervalent cations on the Zr site. Prior experimental observations with Al doping and combination density functional and molecular dynamics computations predict that the critical amount of Li vacancies needed to stabilize the cubic garnet polymorph is 0.4 – 0.5 per LLZO formula unit. These predictions are in agreement for super valent cation doping on the Li site. However, previous reports have suggested that cubic LLZO was stabilized by doping super valent cations on the Zr site with only 0.25 moles of Li vacancies per LLZO formula unit. In order to conclusively determine the concentration of supervalent cations on the Zr required to stabilize cubic LLZO, two Al - free compositions, a critically doped composition of $Li_{6.5}La_3Zr_{1.5}Ta_{0.5}O_{12}$ and a subcritically doped composition of $Li_{6.75}La_3Zr_{1.75}Ta_{0.25}O_{12}$, were investigated. As in prior reports, X-ray diffraction showed both compositions as cubic. However, upon further investigation with other materials characterization techniques including SEM analysis, Raman spectroscopy, electrochemical impedance spectroscopy with equivalent circuit modeling, and neutron diffraction it was evident that $Li_{6.75}La_3Zr_{1.25}Ta_{0.25}O_{12}$, is a mixture of tetragonal and cubic phases. These results confirm: 1) the predictions that a critical doping level of 0.4 – 0.5 Li vacancies per LLZO formula unit is required to stabilize the cubic phase are correct, 2) the previous discrepancies between prediction and the experimental results for super valent cation doping on the Zr site are likely a result of Al incorporated during the processing steps, and 3) when a composition is insufficiently doped to stabilize the cubic polymorph, a mixture of tetragonal and cubic phases results. Furthermore, SEM analysis and Raman spectroscopy can complement X-ray diffraction results and confirm the presence of the tetragonal polymorph in compositions near the critical doping level of 0.4 – 0.5 Li vacancies per formula unit in LLZO garnet solid electrolytes.

Acknowledgements

TT and JS would like to acknowledge support from the Revolutionary Materials for Solid State Energy Conversion, an Energy Frontier Research Center funded by the US Department of Energy, Office of Science, Office of Basic Energy Science under Award Number DE SC001054. JW and JA would like to acknowledge support of the U.S. Army Research Laboratory (ARL). The diffraction Research conducted at the Spallation Neutron Source at Oak Ridge National Laboratory was sponsored by the Scientific User Facilities Division, Office of Basic Energy Sciences, U.S. Department of Energy.

Notes and references

a Michigan State University, Dept. of Chemical Engineering and Materials Science, 2527 Michigan State University, East Lansing, MI 48824.

b Army Research Laboratory, RDRL-SED-C, 2800 Powder Mill Road, Adelphi, MD 20783.

c Naval Research Laboratory, Center for Computational Materials Science, Anacostia, VA.

d Spallation Neutron Source, Oak Ridge National Laboratory, Oak Ridge TN.

Electronic Supplementary Information (ESI) available. See DOI: 10.1039/b000000x/

1 R. Murugan, V. Thangadurai, and W. Weppner, Angew. Chemie Inter. Ed., 2007, **46**, 7778
2 S. Ohta, T. Kobayashi, and T. Asaoka, J. of Power Sources, 2011, **196,** 3342-3345.
3 M. Kotobuki, K. Kanamura, Y. Sato, and T. Yoshida, J. of Power Sources, 2011, **196**, 7750-7754.
4 Y. Shimonishi, A. Toda, T. Zhang, A. Hirano, N. Imanishi, O. Yamamoto, and Y. Takeda, Solid State Ionics, 2011, **183**, 48-53.
5 J. Awaka, N. Kijima, H. Hayakawa, and J. Akimoto, J. of Solid State Chem., 2009, **182**, 2046 – 2052.
6 J. Wolfenstine, E. Rangasamy, J.L. Allen, and J. Sakamoto, J. of Power Sources, 2012, **208**, 193-196.
7 H. Buschmann, J. Dolle, S. Berendts, A. Kuhn, P. Bottke, M. Wilkening, P. Heitjans, A. Senyshyn, H. Ehrenberg, A. Lotnyk, V. Duppel, L. Kienle, and J. Janek, Phys. Chem. Chem. Phys., 2011, **13**, 19378–19392.
8 E. Rangasamy, J. Wolfenstine, and J. Sakamoto, Solid State Ionics, 2012, **206**, 28-32.
9 N. Bernstein, M. D. Johannes, and K. Hoang, Phys. Rev. Lett., 2012, **109**, 205702.
10 C. A. Geiger, E. Alekseev, B. Lazic, M. Fisch, T. Armbruster, R. Langner, M. Fechtelkord, N. Kim, T. Pettke, and W. Weppner, Inorg. Chem., 2010, **50**, 1089-1097.
11 E. Rangasamy, J. Wolfenstine, and J. Sakamoto, Solid State Ionics, 2012, **206**, 28-32.
12 J. Wolfenstine, J. Ratchford, E. Rangasamy, J. Sakamoto, and J. Allen, Mater. Chemistry and Phys., 2012, **134**, 571 – 575.
13 D. Rettenwander, C.A. Geiger, and G. Amthauer, Inorg. Chem., 2013, **52**, 8005-8009.
14 Y. Kihira, S. Ohta, H. Imagawa, and T. Asaoka, ECS Electrochem. Lett., 2013, **2**, A56-A59
15 Logéat, T. Köhler, U. Eisele, B. Stiaszny, A. Harzer, M. Tovar, A. Senyshyn, H. Ehrenberg, and B. Kozinsky, Solid State Ionics, 2012, **206**, 33-38.

16 Y. Li, J.T. Han, C.A. Wang, H. Xie, and J.B. Goodenough, J. of Mater. Chem., 2012, **22**, 15357-15361
17 S. Ramakumar, L. Satyanarayana, S.V. Manorama, and R. Murugan, Phys. Chem. Chem. Phys., 2013, **15**, 11327 - 11338.
18 D. Rettenwander, P. Blaha, R. Laskowski, K, Schwarz, P, Bottke, M. Wilkening, C. A. Geiger, and G. Amthauer, Chem. of Mater., 2014, in press, DOI: 10.1021/cm5000999
19 R.D. Shannon, Acta. Crystallogr., 1976, **751**, A32.
20 R.A. Huggins, Ionics, 2002, **8**, 300-313.
21 F. Tietz, T. Wegener, M.T. Gerhards, M. Giarola, and G. Mariotto, Solid State Ionics, 2012, **230**, 77-82.
22 J. Irvine, D. Sinclair, and A. West, Adv. Mater., 1990, **2**, 132-138.
23 A.K. Ivanov-Schitz and J. Schoonman, Solid State Ionics, 1996, **91**, 93 - 99.
24 T. Fang and C.P. Liu, Chem. of Mater., 2005, **17**, 5167 - 5171.